Homoepitaxial n-core: p-shell gallium nitride nanowires: HVPE overgrowth on MBE nanowires

2011 Nanotechnology 22 465703

(http://iopscience.iop.org/0957-4484/22/46/465703)

Nanotechnology **22** (2011) 465703 (7pp) doi:10.1088/0957-4484/22/46/465703

Homoepitaxial n-core: p-shell gallium nitride nanowires: HVPE overgrowth on MBE nanowires

Aric Sanders[1], Paul Blanchard[1], Kris Bertness[1], Matthew Brubaker[1], Christopher Dodson[1], Todd Harvey[1], Andrew Herrero[1], Devin Rourke[1], John Schlager[1], Norman Sanford[1], Ann N Chiaramonti[2], Albert Davydov[2], Abhishek Motayed[2] and Denis Tsvetkov[2]

[1] National Institute of Standards and Technology, Physical Measurement Laboratory, 325 Broadway, Boulder, CO 80305, USA
[2] National Institute of Standards and Technology, Material Measurement Laboratory, 100 Bureau Drive, Gaithersburg, MD 20899, USA

E-mail: aric.sanders@nist.gov

Received 29 June 2011, in final form 23 September 2011
Published 25 October 2011
Online at stacks.iop.org/Nano/22/465703

Abstract
We present the homoepitaxial growth of p-type, magnesium doped gallium nitride shells by use of halide vapor phase epitaxy (HVPE) on n-type gallium nitride nanowires grown by plasma-assisted molecular beam epitaxy (MBE). Scanning electron microscopy shows clear dopant contrast between the core and shell of the nanowire. The growth of magnesium doped nanowire shells shows little or no effect on the lattice parameters of the underlying nanowires, as measured by x-ray diffraction (XRD). Photoluminescence measurements of the nanowires show the appearance of sub-bandgap features in the blue and the ultraviolet, indicating the presence of acceptors. Finally, electrical measurements confirm the presence of electrically active holes in the nanowires.

(Some figures in this article are in colour only in the electronic version)

1. Introduction

Nanowire growth of the III–V semiconductors, in particular the III-nitrides, has exploded in the last decade due to the prospect of solving longstanding growth issues in these material systems. Nanowires offer the ability to grow high-quality single crystals of AlN, InN, and GaN at predetermined locations and sizes [1–3]. This growth is independent of lattice mismatches of the underlying substrate. In particular, the strain and resulting high defect density that plagues film growth is almost non-existent in nanowire growth. In addition, the ability to control morphology and composition to an almost arbitrary degree has been demonstrated repeatedly [4]. These factors make nanowires grown from GaN and its related alloys very promising for high-efficiency single nanowire light emitting diodes (LEDs). Single nanowire LEDs could lead to an array of new integrated technologies including but not limited to near-field scanning optical microscopy (NSOM) sources, light sources for Si microelectronics, and low-power microfluidic-based water purification systems. To accomplish the highest-efficiency single nanowire emitters, a complex array of device and material engineering issues must be simultaneously addressed. Catalyzed growth of GaN nanowires is popular for the flexibility it provides; however, catalyst contamination or carbon incorporation from organometallic precursors still may limit the quality of GaN nanowires. In particular, the most promising growth techniques, such as organometallic vapor phase epitaxy and hot-wall chemical vapor deposition, show sub-gap photoluminescence (PL) [2], and high intrinsic carrier concentrations [5]. To overcome these difficulties, we use nitrogen plasma-assisted molecular beam epitaxy (MBE). The slow growth rate allows for superb control over axial doping profiles and wire composition [6]. Additionally, the quality of material has been shown to be excellent by

many researchers [6–9]. However, the radial incorporation of magnesium while simultaneously optimizing wire morphology has yet to be realized for MBE growth. This is because of the small latitude in process parameters to attain adequate Mg incorporation via MBE. To overcome this limitation, while taking advantage of the high material quality of the MBE growth method, it is important to investigate two-stage growths. In particular, use of MBE nanowires as a strain-free low defect density scaffold for other growth methods is promising. A popular choice of growth methods for commercial thin-film GaN is halide vapor phase epitaxy (HVPE). HVPE provides high growth rates and reproducible p-doped layers. We present the growth of a Mg:GaN shell by use of HVPE on n-type nanowires grown by use of plasma-assisted MBE.

2. Growth

The *c*-axis, catalyst-free nanowire cores were grown by use of plasma-assisted MBE [10]. Wires were grown on Si(111) substrates that were prepared by HF etch (10% HF:H20) and oxide desorption steps at 750 °C for 15 min and then 850 °C for 10 min. After this pretreatment, a thin (<1 nm) aluminum wetting layer was deposited at 700 °C. Next, an AlN buffer layer approximately 75 nm thick was grown by use of a solid source Al effusion cell, and a radio frequency nitrogen plasma source at a substrate temperature of 630 °C. Finally, wires were grown at temperatures between 800 and 850 °C, under high nitrogen flux conditions, to a length of 5–15 μm, with diameters ranging from 50 to 500 nm. In addition to nanowires, as-grown material includes a shorter 'matrix' layer of highly faceted material surrounding the nanowire roots. This matrix layer frequently includes a high density of basal stacking faults [10]. Five growths of such GaN wires were used for this study: three growths of undoped nanowires with room-temperature n-type carrier concentrations of 10^{15}–10^{16} cm^{-3} (B992, B822, B738) and two growths of intentionally silicon doped wires with carrier concentrations of 10^{17}–10^{18} cm^{-3} (B982, C023). Carrier concentrations were measured by correlating nanowire resistance with nanowire dimensions and modulating the depleted region of nanowires made into two-terminal electrical devices [11, 12] by use of ultraviolet light exposure. After growth of the nanowires, the p-type GaN shells were deposited on a piece of as-grown MBE nanowire material in an HVPE reactor. HVPE was chosen for its proven ability to grow high carrier concentration p-type material and the lack of any hydrocarbon precursors. The HVPE reactor is of standard design with HCl being flowed over molten Ga to create GaCl that is delivered to the substrate by use of nitrogen as a carrier gas [13]. The source of reactive nitrogen for the growth of GaN was NH_3 at flow rates of ~2000 sccm. Typical growth temperatures were 900–1000 °C, causing the wires to quickly grow, at ~200 nm min^{-1}, in diameter with typical growth periods of 3 min or less and the thickness of coatings ranging from 50 to 600 nm, for total coated wire diameters of 100 nm–1 μm. Thin-film samples grown under similar conditions show atomic magnesium doping concentrations of 4 × 10^{19} cm^{-3} as determined by secondary ion mass spectrometry (SIMS); see figure 1.

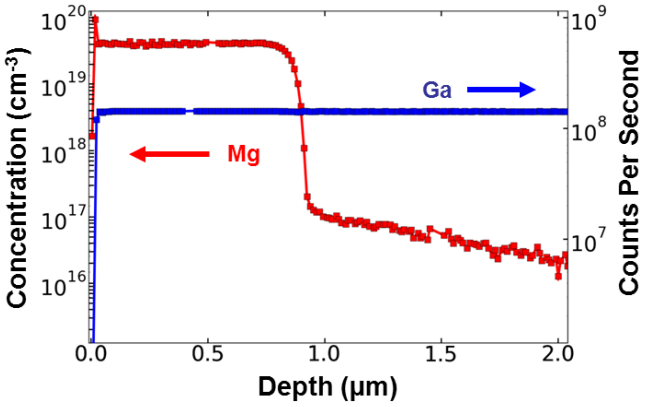

Figure 1. SIMS of a reference film. SIMS shows a concentration of Mg atoms of 4 × 10^{19} cm^{-3} (red curve, left axis), for 1.42 × 10^{8} Ga counts s^{-1} (blue curve, right axis) for a film grown under equivalent conditions to the nanowire growths. The growth time of the film was slightly longer to provide more material for characterization (total thickness of Mg doped GaN was ~1 μm).

After growth, the wires are inspected for changes in morphology in a field-emission scanning electron microscope (FESEM). Secondary electron imaging reveals a clear contrast between the core and shell in all of the unintentionally doped nanowires; see figure 2. This contrast is consistent with doping contrast seen in Si [14]. It appears strongest for low acceleration voltages and in-lens type detectors, indicating that the information regarding dopant concentration is carried by the secondary electrons generated by the primary beam and not by the high-energy back-scattered electrons. This technique reveals inhomogeneity in the dopant distribution of the resulting core–shell nanowire structure. First, cores are not always concentric with the shells (approximately 30% in a representative sample of 85 wires). Second, the shells are of varying thickness, with the range of shell thicknesses for a representative sample being 50–200 nm. And finally, we observe apparent growth anisotropy for the *c*-face of the nanowires, or the HVPE overgrowth appears thinner on the *c*-plane. Since this technique is sensitive to electric fields generated by dopant distributions, the relative ratio of how much of this is caused by a differential growth rate between the *m*-plane and *c*-plane and how much is caused by dopant diffusion in the overgrowth process is still unknown.

In contrast to FESEM, transmission electron micrographs show no dopant-based contrast in either bright-field or conventional dark-field imaging. Figure 3 shows transmission electron micrographs of a wire from a growth that showed clear dopant contrast in FESEM images. In addition to the lack of dopant contrast, the TEM micrographs show a lack of extended defects. The dark-field image formed by imaging with the $(2\,\bar{1}\,0)$ diffraction spot also shows no cracking or large defects with lattice distortions with components in the *g* direction. The selected area electron diffraction (SAED) image (inset on top left), together with the corresponding images indicate that the wire has no crystallographic twinning [15] driven by HVPE re-growth; we believe that the small satellite spots present in the

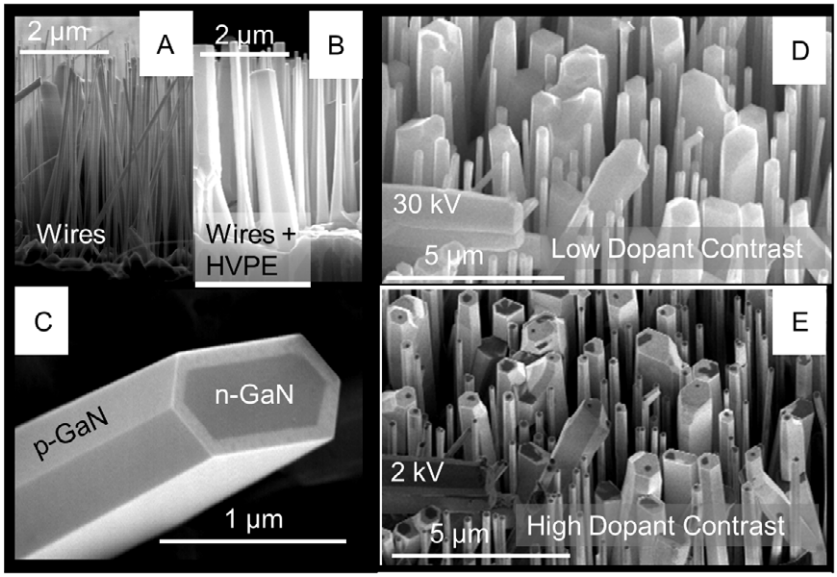

Figure 2. Scanning electron micrographs of n-type MBE nanowires with HVPE p-type shells. (A) A cross section of n-type MBE nanowire cores before HVPE overgrowth. (B) A cross section after the growth of a p-type HVPE shell. (C) A single core–shell nanowire that shows clear contrast between n-type and p-type materials. (D) A large sample of core–shell nanowires imaged at 45° to the normal, in a low-contrast condition, i.e. large acceleration voltage with an Everhart–Thornley detector (bias +100 V). (E) A large sample of core–shell nanowires imaged at 45° to the normal, in a high-contrast condition, i.e. low acceleration voltage with an in-lens detector.

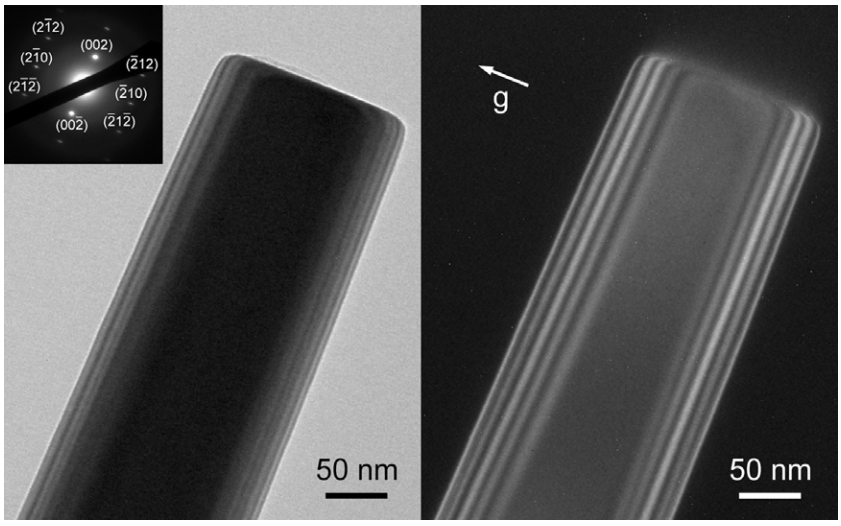

Figure 3. Transmission electron micrograph of a core–shell nanowire (GN84). Bright-field transmission electron micrograph (left) showing no observable defects and thickness fringes. Dark-field electron micrograph $g = (2\,\bar{1}\,0)$, also showing no observable defects and thickness fringes. SAED pattern (inset) illustrating the single-crystal nature of the wires.

diffraction pattern arise from the thickness fringes of the edges of the wedge-shaped hexagonal-crystal habit. Although no large defects were visible in a single nanowire, it is important to determine the strain state of an ensemble of wires before and after growth of the homoepitaxial shell.

3. X-ray

In order to establish the effect of homoepitaxial growth on the nanowires, x-ray diffraction patterns of samples with and without HVPE growth were taken. A total of six samples, three without HVPE growth (B738, C023, B982) and three with (GN84, GN169, GN97) were analyzed. Each sample of wires remained affixed to a Si(111) substrate with a ∼75 nm AlN buffer layer, and no attempt was made to separate the reflections from the matrix layer and the wires. For each sample, six reflections were taken in the two-theta direction, three symmetric, and three asymmetric, by use of a high-resolution x-ray diffractometer. The source of x-rays was filtered by selecting the copper Kα_1 line at 0.154 0595 nm. Table 1 summarizes the x-ray reflection peak positions and full width at half maxima (FWHM) for each sample and reflection.

The peak positions of the symmetric reflections (002, 004, 006) were used to calculate the c lattice parameter for

Table 1. 2θ–ω diffractions of gallium nitride nanowires. X-ray reflections of nanowires before and after HVPE overgrowth used in calculating lattice parameters. The reported 2θ is the restricted range centroid, taking the weighted average of the values between half maximum points, along with the full width at half maximum (FWHM). For a given sample, all of the symmetric reflections are used to calculate an average c lattice parameter. This c lattice parameter is used with the asymmetric reflections to calculate the average a lattice parameter.

Symmetric diffractions							
		002		004		006	
Description	Sample	2θ angle (deg)	FWHM (deg)	2θ angle (deg)	FWHM (deg)	2θ angle (deg)	FWHM (deg)
Wires	B738	34.575	0.029	72.928	0.067	126.125	0.196
HVPE on B738 wires	GN84	34.574	0.042	72.926	0.092	126.126	0.256
Repeat of GN84	GN84b	34.570	0.042	72.920	0.093	126.117	0.252
Wires	C023	34.570	0.014	72.919	0.035	126.099	0.120
HVPE on C023 wires	GN169	34.564	0.025	72.914	0.039	126.095	0.120
Wires	B982	34.572	0.015	72.925	0.037	126.115	0.130
HVPE on B982 wires	GN97	34.571	0.020	72.924	0.044	126.114	0.140
Asymmetric diffractions							
		104		105		204	
Description	Sample	2θ angle (deg)	FWHM (deg)	2θ angle (deg)	FWHM (deg)	2θ angle (deg)	FWHM (deg)
Wires	B738	82.065	0.342	105.032	0.257	109.173	0.460
HVPE on B738 wires	GN84	82.046	0.109	105.023	0.219	109.145	0.204
Repeat of GN84	GN84b	82.051	0.116	105.029	0.219	109.151	0.206
Wires	C023	82.049	0.086	105.011	0.103	109.166	0.139
HVPE on C023 wires	GN169	82.050	0.062	105.015	0.094	109.183	0.099
Wires	B982	82.065	0.071	105.030	0.103	109.198	0.127
HVPE on B982 wires	GN97	82.062	0.082	105.026	0.117	109.187	0.148

each sample. The average of these measurements yielded a value of c lattice parameter that was used with the asymmetric reflections (104, 105, 204) to calculate the a lattice parameter. This method is explained in detail in [16]. Each peak position was determined by finding the weighted average of the points from half maximum to half maximum, i.e. a restricted range centroid. In order to track the stability of x-ray measurements, one as-grown specimen had reflections taken by separate users after a long period (∼5 months), these reflections are reported as GN87 and GN87b. This repeated experiment places a reasonable estimate on all errors associated with sample misalignment, long-term environmental changes such as humidity, temperature, and general operator differences of at most $\pm 6 \times 10^{-5}$ (120 ppm) fractionally and typically $\pm 3 \times 10^{-5}$ (60 ppm). These errors are similar to the fractional errors assigned by use of the internal variation of the lattice parameters calculated for each reflection. Since each 2θ–ω scan of a reflection constitutes a separate measurement of the c lattice, it is reasonable to expect that the error in the mean value of the lattice parameters will be representative of the precision of the measurement. With this in mind, the errors in the lattice parameters are assigned by taking the 95% confidence interval for the mean of c lattice values, to a maximum fractional accuracy of 120 ppm, and then repeating this for the a lattice values calculated from the mean c lattice for each sample. The average c lattice parameter for all of the samples in this study is between 0.518 53 and 0.518 43 nm, and the a lattice parameters are between 0.3188 and 0.3192 nm. Although the x-ray reflections were the result of both the matrix and the nanowires, the measured lattice parameters agree very well with measurements of the strain-free values of GaN found in the literature. To illustrate this point, a range of strain-free GaN lattice parameters found in the literature is represented by a gray box in figure 4. The box is formed by [17] and [18], forming a range of values in which most reported values for strain-free lattice parameters are included; a summary of many of the values appears in [16]. In addition, figure 4 illustrates that the addition of the HVPE p-type material does not affect the average lattice parameter of the nanowires. This is consistent with bulk homoepitaxy [17] that shows no change in lattice parameters regardless of Mg doping, within the resolution of our experiment.

4. Photoluminescence

Although Mg incorporation had no measurable effect on lattice parameters, the presence of an acceptor in single nanowires is evident in PL spectra. PL of single nanowires removed from the growth substrate were measured in a continuous flow helium cryostat, by use of a HeCd laser as an excitation source. To prepare samples for PL measurements at 5 K, a large number of wires were released from the growth substrate by ultrasonic agitation in isopropanol to produce a suspension. This suspension was dried on a fused-silica substrate with a photolithographically defined, indexed metal grid to aid in the identification and location of individual wires. UV emission from the HeCd laser (325 nm) was focused onto the sample through a fused-silica window in the cryostat. The resultant PL spectra were obtained with a scanning 0.5 m monochromator that collected and dispersed the luminescence onto an UV-sensitive photomultiplier tube. The PL collected is a weighted

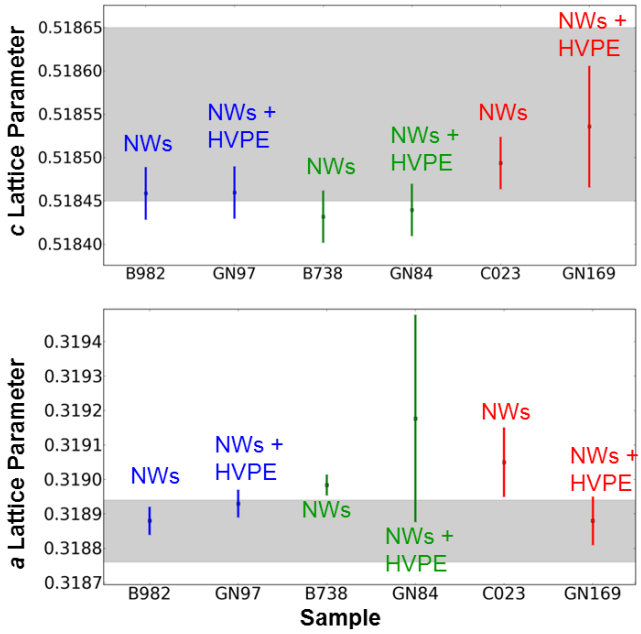

Figure 4. GaN nanowire lattice parameters measured by XRD. Lattice parameters undergo no significant change before and after HVPE growth of p-type shells. The gray region represents literature values for strain-free GaN. The x-ray reflections used in determining the lattice constants and their errors are presented in table 1.

sum of GaN perpendicular to the incidence of the beam to a depth of approximately 80 nm [19]. Any variation in thickness of the nanowire, or film coating the nanowire, will serve to generate an average spectrum. The PL spectra of MBE nanowire cores have distinct band-edge emission due to the donor bound A-exciton (D^0X_A) at 3.472 eV. Occasionally, this peak will be displaced by up to ∼15 meV due to strain induced by the differential thermal contraction between the GaN and the substrate [20]. For the nanowire cores it is common to observe up to four phonon replicas of the emission from exciton transitions in the spectra, which are spaced at regular intervals determined by the longitudinal optical (LO) phonon energy (∼92 meV). Single nanowires have no significant yellow emission or any other significant sub-bandgap emission. In contrast, once the HVPE shell is grown there are at least two recognizable sub-bandgap features. At 5 K, these features occur roughly at 2.9 and 3.25 eV and can be seen in figure 5, for two coated nanowire growth runs. These features are broad and occur typically in spectral regions and can be associated with various acceptors. The blue luminescence (BL) band has been observed in unintentionally doped, Zn, and Mg doped GaN grown by HVPE, and we use the notation found in [21]. Since we have intentionally introduced Mg, and have analyzed thin films grown in similar conditions using SIMS, we believe that the BL band is caused by Mg incorporated into the overgrowth of GaN on the nanowire. In addition, although the ultraviolet luminescence (UVL) band occurs close to the same spectral position as the 2 LO phonon replica of the exciton transitions, we believe the vastly increased magnitude and the broadening of features at approximately 3.25 eV represent the incorporation of Mg. The difference in shape for the overcoated wires labeled GN84 and GN97 occurs most likely because of a difference in concentration of Mg. Others have reported that at a certain doping level the peaks of the UVL band broaden, redshift, and transform into a single unstructured band peaking at about 3.2 eV [21].

5. Electrical characterization

The electrical resistivity and carrier polarity of the core–shell nanowires were determined by two-terminal electrical measurements. Nanowires were first released from their growth substrates by ultrasonic agitation in isopropanol. The wire suspension was then deposited on fused-silica substrates and metallic leads were patterned and deposited by use of standard lift-off photolithographic techniques. A large number of electrode pairs are patterned and a small fraction result in single nanowire devices; several different contacting metals and annealing schemes were tested. Comparing the current that flows through unintentionally doped nanowires before and after HVPE growth, it is clear that the HVPE film is conductive. All HVPE overgrown wire growths were conductive regardless of their initial resistivity. For example, wires from the B992 growth have an estimated carrier concentration of $\sim 10^{15}$ cm^{-3} and are completely depleted at room temperature. Measurements of 25 devices with single wires clearly bridging electrode pairs, and 50 nm Ni/292 nm

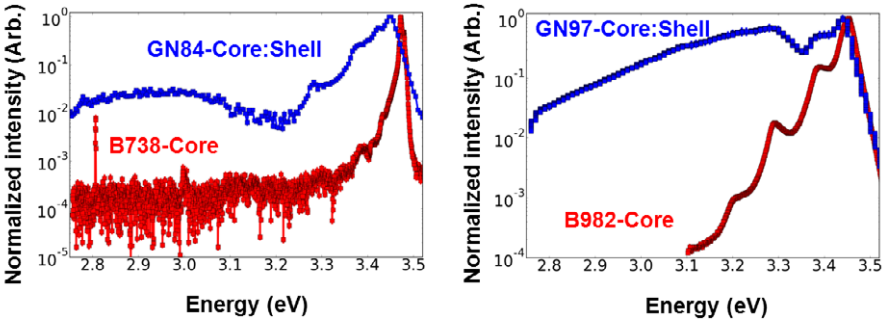

Figure 5. PL at 5 K of single wires from the growths B982 and B738 for both n-type single nanowires and core–shell n–p nanowires. In both cases an increase of sub-bandgap spectral content indicates the presence of an acceptor. At 5 K, two donor–acceptor pair (DAP) transitions are apparent in core–shell nanowires, but not in MBE nanowire cores. These transitions are referred to as BL and UVL, to correspond to the bulk equivalents reported in [21].

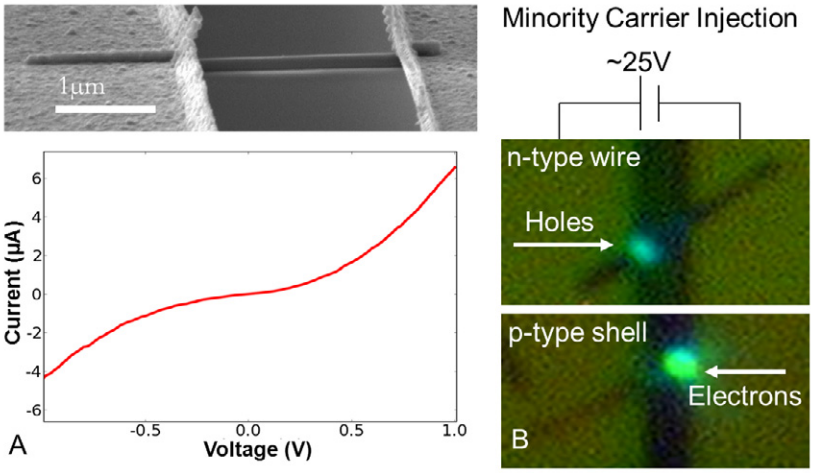

Figure 6. Electrical measurements. (A) A typical core–shell device micrograph with Ni/Au contacts. The core nanowires are B992 and are completely depleted at room temperature. There has been no attempt in this device to contact the core selectively. A typical current–voltage curve of a comparable device is shown directly below. Non-ohmic device characteristics are typical in core–shell devices for both n-type and p-type contact metallization schemes. (B) Minority carrier injection from the metallic contacts. In the case of n-type nanowire cores (top) holes are injected, causing electroluminescence to appear next to the positively biased lead, whereas in the case of core–shell nanowires contacted only on the shell (bottom), electrons are injected, causing electroluminescence near the negatively biased lead.

Au contacts, unannealed, show virtually no conduction, and current–voltage curves in all instances have currents less than 10^{-10} A at 1 V, a system noise floor for fast characterization. In contrast, after the HVPE growth, a sample with the same contact metallization, shows the wires are conductive, having a typical current of 10^{-6} A at 1 V. Of 17 devices measured, each clearly having a single wire between the electrode pairs, 16 had currents at 1 V that ranged between 10^{-5} and 10^{-10} A. The inhomogeneity in the shell dimensions no doubt plays a role in the large distribution of currents at 1 V. The current–voltage characteristics of devices are predominately nonlinear, having a barrier associated with the contact, a typical device micrograph and a typical current–voltage curve is shown in figure 6(A).

This is true regardless of the contact metallization, whether it is 20 nm Ti/200 nm Al or 50 nm Ni/292 nm Au, and generally nanowire contacts worsen under contact annealing. In contrast, contacts to n-nanowires with annealed Ti/Al contacts are normally linear and of low resistance [11]. This is qualitatively consistent with the increase in contact barrier associated with p-doping; however, it is not conclusive. This change in contact quality was observed for all of the HVPE overcoated growth runs. For certain devices that can tolerate high applied voltages >25 V and have currents that exceed 10^{-7} A at 25 V, mild electroluminescence from single wires is observed. The visible part of this electroluminescence is dim and requires camera integration times of 10–20 s to capture; see figure 6(B). Wires with p-type material tend to emit light close to the negatively biased lead, whereas n-type wires, with no p-type material, emit close to the positively biased lead. This type of polarity dependent light emission is seen when minority carriers are extracted from the metallic leads and injected into semiconductors [22]. It should be noted that minority carriers injected from the metal contacts can either directly tunnel into the semiconductor or have sufficient kinetic energy to impact ionize lattice atoms, creating a minority carrier population with a small fraction that recombines radiatively. We do not observe a significant increase in current for biases greater than that at which the luminescence is observed, suggesting that the avalanche generation of carriers is not dominating the current characteristics. The polarity of this effect indicates that there are electrically active holes in the p-type material.

6. Conclusion

In conclusion, using n-type nanowires grown by MBE and a p-type cladding grown by HVPE, we have demonstrated the growth of homoepitaxial n-core:p-shell nanowires. These wires have clear signatures of dopant contrast in scanning electron micrographs, no apparent defects in electron diffraction patterns and TEM images, and a clear PL signature related to an acceptor in the HVPE shell. In addition, no change in lattice parameter is observed for large ensembles of nanowires as measured by x-ray diffraction indicating homoepitaxial growth. Finally, active holes in the coated wires are observed through minority carrier tunneling electroluminescence.

Acknowledgments

We would like to acknowledge Dr Manuel Romero for many useful discussions and data regarding cathode-luminescence in similar structures. This is a contribution of an agency of the US government and is not subject to copyright.

References

[1] Hersee S, Sun X and Wang X 2006 The controlled growth of GaN nanowires *Nano Lett.* **6** 1808–11

[2] Ishizawa S, Sekiguchi H, Kikuchi A and Kishino K 2007 Selective growth of GaN nanocolumns by Al thin layer on substrate *Phys. Status Solidi* b **244** 1815–9
[3] Bertness K A, Sanders A W, Rourke D M, Harvey T E, Roshko A, Schlager J B and Sanford N A 2010 Controlled nucleation of GaN nanowires grown with molecular beam epitaxy *Adv. Funct. Mater.* **20** 2911–5
[4] Qian F, Gradecjak S, Li Y, Wen C-Y and Lieber C 2005 Core/multishell nanowire heterostructures as multicolor, high-efficiency light-emitting diodes *Nano Lett.* **5** 2287–91
[5] Stern E *et al* 2005 Electrical characterization of single GaN nanowires *Nanotechnology* **16** 2941–53
[6] Calleja E *et al* 2007 Growth, morphology, and structural properties of group-III-nitride nanocolumns and nanodisks *Phys. Status Solidi* b **244** 2816–37
[7] Tchernycheva M *et al* 2007 Growth of GaN free-standing nanowires by plasma-assisted molecular beam epitaxy: structural and optical characterization *Nanotechnology* **18** 385306
[8] Guo W, Zheng M, Banerjee A and Bhattacharya P 2010 Catalyst-free InGaN/GaN nanowire light emitting diodes grown on (001) silicon by molecular beam epitaxy *Nano Lett.* **10** 3355–9
[9] Calarco R and Marso M 2007 GaN an InN nanowires grown by MBE: a comparison *Appl. Phys.* A **87** 499–503
[10] Bertness K, Roshko A, Mansfield L, Harvey T and Sanford N 2007 Nucleation conditions for catalyst-free GaN nanowires *J. Cryst. Growth* **300** 94–9
[11] Mansfield L, Bertness K, Blanchard P, Harvey T, Sanders A and Sanford N 2009 GaN nanowire carrier concentration calculated from light and dark resistance measurements *J. Electron. Mater.* **38** 495–504
[12] Sanford N, Blanchard P, Bertness K, Mansfield L, Schlager J, Sanders A, Roshko A, Burton B and George S 2010 Steady-state and transient photoconductivity in *c*-axis GaN nanowires grown by nitrogen-plasma-assisted molecular beam epitaxy *J. Appl. Phys.* **107** 034318
[13] Ambacher O 1998 Growth and applications of group III-nitrides *J. Phys. D: Appl. Phys.* **31** 2652–710
[14] El-Gomati M, Zacjgout F, Jayacody H, Tear S and Wilson K 2005 Why is it possible to detect doped regions of semiconductors in low voltage SEM: a review and update *Surf. Interface Anal.* **37** 907–11
[15] Wiliams D and Carter C 2009 *Transmission Electron Microscopy: A Textbook for Materials Science* 2nd edn (Berlin: Springer)
[16] Moram M and Vickers M 2009 X-ray diffraction of III-nitrides *Rep. Prog. Phys.* **72** 036502
[17] Porowski S 1998 Bulk and homoepitaxial GaN-growth and characterisation *J. Cryst. Growth* **190** 153–8
[18] Leszcznski M, Grzegory I, Teisseyre H, Suski T, Bockowski M, Jun J, Branowski J M, Poroski S and Major J 1995 Lattice constants, thermal expansion and compressibility of gallium nitride *J. Phys. D: Appl. Phys.* **28** A149
[19] Muth J, Lee J, Shmagin I, Kolbas R, Casey H, Keller B, Mishra U and DenBaars S 1997 Absorbtion coefficient, energy gap, exciton binding energy, and recombination lifetime of GaN obtained from transmission experiments *Appl. Phys. Lett.* **71** 2572–4
[20] Schlager J, Bertness K, Blanchard P, Robins L, Roshko A and Sanford N 2008 Steady-state and time-resolved photoluminescence from relaxed and strained GaN nanowires grown by catalyst-free molecular-beam epitaxy *J. Appl. Phys.* **103** 124309
[21] Reshchikov M and Morkoc H 2005 Luminescence properties of defects in GaN *J. Appl. Phys.* **97** 061301
[22] Zimmler M, Bao J, Shalish I, Yi W, Yoon J, Narayanamurti N and Capasso F 2007 Electroluminescence from single nanowires by tunnel injection: an experimental study *Nanotechnology* **18** 235205